ACS PHYSICAL CHEMISTRY Au
AN OPEN ACCESS JOURNAL OF THE AMERICAN CHEMICAL SOCIETY

pubs.acs.org/physchemau Article

Release of a Proton and Formation of a Low-Barrier Hydrogen Bond between Tyrosine D and D2-His189 in Photosystem II

Manoj Mandal, Keisuke Saito, and Hiroshi Ishikita*

Cite This: ACS Phys. Chem Au 2022, 2, 423−429 Read Online

ACCESS | Metrics & More | Article Recommendations | Supporting Information

ABSTRACT: In photosystem II (PSII), the second-lowest oxidation state (S_1) of the oxygen-evolving Mn_4CaO_5 cluster is the most stable, as the radical form of the redox-active D2-Tyr160 is considered to be a candidate that accepts an electron from the lowest oxidation state (S_0) in the dark. Using quantum mechanical/molecular mechanical calculations, we investigated the redox potential (E_m) of TyrD and its H-bond partner, D2-His189. The potential energy profile indicates that the release of a proton from the TyrD...D2-His189 pair leads to the formation of a low-barrier H-bond. The E_m depends on the H^+ position along the low-barrier H-bond, e.g., 680 mV when the H^+ is at the D2-His189 moiety and 800 mV when the H^+ is at the TyrD moiety, which can explain why TyrD mediates both the S_0 to S_1 oxidation and the S_2 to S_1 reduction.

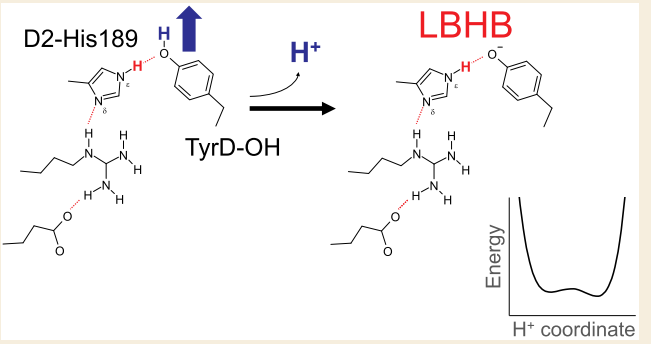

KEYWORDS: *low-barrier hydrogen bond, redox-active tyrosine, histidine radical, delocalized H-bond network, proton-coupled electron transfer, oxygen-evolving complex, dark adaptation, photoactivation*

INTRODUCTION

Oxygen evolution occurs at the catalytic Mn_4CaO_5 cluster in photosystem II (PSII), removing four electrons and four protons from two substrate water molecules. To oxidize the water molecules, the electron transfer pathway proceeds from the Mn_4CaO_5 cluster via a H-bond pair, the redox-active tyrosine (TyrZ) and D1-His190, toward chlorophyll $[P_{D1}/P_{D2}]^{\bullet+}$ (Figure 1). As electron transfer occurs, the oxidation state of the Mn_4CaO_5 cluster, S_n, increases from S_0 to S_3 via S_1 and S_2: $S_0 \rightarrow S_1 \rightarrow S_2 \rightarrow S_3 \rightarrow S_0$ (e.g.,[1,2]), and O_2 evolves in the S_3-to-S_0 transition. In the proton-coupled electron transfer, the neutral radical $TyrZ^{\bullet}$ is transiently formed upon oxidation of TyrZ by $[P_{D1}/P_{D2}]^{\bullet+}$ on a timescale of tens to hundreds of nanoseconds in intact PSII.[3,4]

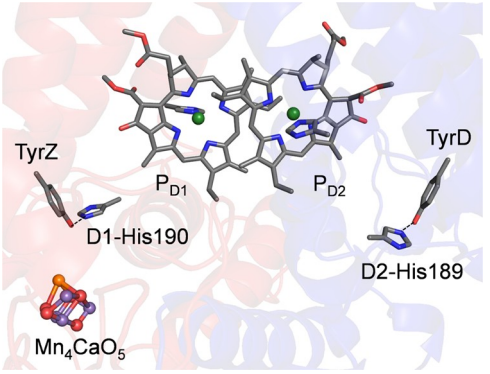

Figure 1. Redox-active groups on the lumenal side of PSII. Dotted lines indicate H-bonds for the tyrosine−histidine pairs.

TyrZ forms an unusually short (2.46 Å[5]) low-barrier H-bond with Nε of D1-His190,[6] facilitating proton-coupled electron transfer.[6,7] Low-barrier H-bonds can form only when the pK_a values of the H-bond donor and acceptor moieties are nearly equal.[8−10] The H^+ can be delocalized along the low-barrier H-bond, whereas the redox potential[11] and absorption wavelength[12] change in response to the H^+ movement. This does not necessarily mean that these values fluctuate in the proteins, as low-barrier H-bonds often appear in the transition intermediate states (e.g., during the photocycles in microbial rhodopsins and photoreceptors[12,13]). The low-barrier H-bond formation is observed when proton transfer occurs in PSII, e.g., TyrZ and D1-His190,[6,7] Q_B and D1-His215,[14] a ligand water molecule (W1) of the Mn_4CaO_5 cluster and D1-Asp61,[15,16] and the O4 site of the Mn_4CaO_5 cluster and the O4−water chain.[17,18]

Received: March 25, 2022
Revised: May 14, 2022
Accepted: May 16, 2022
Published: May 30, 2022

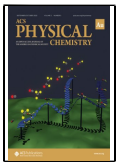

https://doi.org/10.1021/acsphyschemau.2c00019
ACS Phys. Chem Au 2022, 2, 423−429

In contrast, the H-bond distance between D2-Tyr160 (TyrD) and D2-His189 on the D2 side is longer (2.74 Å in the crystal structure).[5] TyrD is not involved in the electron transfer pathway from the Mn_4CaO_5 cluster. However, the neutral deprotonated radical TyrD-O$^\bullet$ is formed upon oxidation of TyrD-OH by $[P_{D1}/P_{D2}]^{\bullet+}$[19−22] and this occurs in a tens of ms timescale[23] (also see ref 24). The proton released from TyrD-OH is transferred along the downhill proton transfer pathway that proceeds via D2-Arg180 and a series of waters toward D2-His61, the protein bulk surface.[25−27] Thus, once formed, TyrD-O$^\bullet$ is highly stable for several hours.[19,21] This suggests that normal enzyme activity occurs in the presence of the tyrosine radical.[21] TyrD-O$^\bullet$ was also observed in the D2-His189 mutant proteins,[28,29] which confirms that TyrD is redox-active. In response to the TyrD-O$^\bullet$ formation, a water molecule, which accepts a H-bond from TyrD-OH (i.e., proximal water-binding position), moves toward D2-Arg180 (i.e., distal water-binding position).[5,25] In the dark-adapted PSII crystal structure, the water molecule is observed at both the proximal and distal positions,[30] which indicates that TyrD-OH and TyrD-O$^\bullet$ coexist.

It has been considered that TyrD-O$^\bullet$ serves as an electron acceptor from S_0 in the dark and is the component that stabilizes the second-lowest oxidation state of the Mn_4CaO_5 cluster, S_1, rather than the lowest oxidation state, S_0 (e.g.,[21]). Long adaptation of PSII to the darkness results in the oxidation of S_0 to S_1 via electron transfer from S_0 to TyrD-O$^\bullet$.[21,31,32] In pea thylakoids, S_0 disappears in ∼20 min.[31] On the other hand, TyrD-O$^-$ donates the electron to S_2, reducing it to S_1 in the dark.[21,32] TyrD-O$^\bullet$ could be formed in the seconds timescale upon illumination[33] because higher S-states (e.g., S_2 and S_3) are formed upon illumination and then reduced to S_1 upon oxidation of TyrD-OH to TyrD-O$^\bullet$.[34] This was confirmed by the two-flash-illuminated structure (S_3: 46%).[30] Based on the negative peak at the proximal water-binding position in the two-flash-minus-dark isomorphous difference Fourier map, Suga et al. reported that the water molecule moves toward the distal binding position, forming TyrD-O$^\bullet$,[30] as originally suggested in theoretical studies by Saito et al.[25]

Thus, the presence of TyrD is likely to be associated with S_1 being the most stable oxidation state in PSII. Based on these findings, it seems plausible to assume that $E_m(S_0/S_1) < E_m(\text{TyrD}) < E_m(S_2/S_1)$.[35] Using the PSII crystal structure and solving the linear Poisson−Boltzmann equation, it was reported that E_m(TryD) is 690 mV, which is >200 mV lower than E_m(TyrZ).[36] The difference between E_m(TyrZ) and E_m(TyrD) is due to the difference in the protonation state of the H-bond partner D1-Asn298, which allows D1-His190 to protonate at the Nδ site, or D2-Arg294, which does not allow D2-His189 to protonate at the Nδ site.[36] The calculated E_m difference between E_m(TyrZ) and E_m(TyrD) is consistent with the experimentally estimated E_m difference of 240 mV.[37] Similar values for E_m(TyrD) and E_m(TyrZ) have also been obtained using a quantum mechanical/molecular mechanical (QM/MM) approach based on the PSII crystal structure.[38] This approach also allows the calculation of the E_m for the Mn_4CaO_5 cluster based on the molecular orbital energy levels. However, among the calculated E_m values, E_m(TyrD) is the lowest (680 mV), even lower than $E_m(S_0/S_1)$ (730 mV).[38] The low E_m(TyrD) value is due to the absence of the protein electrostatic environment that can increase E_m(TyrD-O$^{\bullet/-}$) (note: E_m(Tyr-O$^{\bullet/-}$) = 680 mV in water[39]). If the TyrD...D2-His189 H-bond is a low-barrier H-bond, electron transfer may be pronounced, altering the E_m value in response to the H^+ movement.[11] That is, both the Tyr and His moieties ultimately contribute to the redox activity of the Tyr...His H-bond. However, the TyrD...D2-His189 H-bond is not a low-barrier H-bond in the redox/protonation state of the crystal structure.[25] It is unclear how $E_m(S_0/S_1) < E_m(\text{TyrD}) < E_m(S_2/S_1)$[35] can be explained in terms of the PSII protein environment of the reported PSII crystal structures. Here, we specifically focused on TyrD and re-examined the factors that affect E_m(TyrD) in the PSII protein environment, using a QM/MM approach based on the PSII crystal structure.

METHODS

The atomic coordinates of PSII were obtained from the PSII crystal structure (PDB code, 3ARC).[5] The atomic charges of the other cofactors in the MM region were taken from a previous study.[40]

E_m Calculations

The highest occupied molecular orbital (HOMO) energy level is largely correlated with E_m for one-electron oxidation (e.g.,[41,42]), whereas the lowest unoccupied molecular orbital (LUMO) energy level is largely correlated with E_m for one-electron reduction (e.g.,[43]). We included all redox-active cofactors (Mn_4CaO_5 cluster, TyrZ, P_{D1}, and P_{D2}) simultaneously in the QM region[44,45] (see below), identified HOMOs of Mn_4CaO_5, TyrZ, P_{D1}, and P_{D2} in S_1 on the basis of the Mulliken population analysis[46] (results provided in a previous study[38]), and obtained the E_m values. The E_m values of the redox sites are calculated using eq 1

$$E_m = -0.15499E_{HOMO} + 1205.65 \quad (1)$$

where E_{HOMO} is the HOMO energy level (meV).[11,38,47] Although eq 1 was obtained only assuming that E_m(TyrD) = 680 mV and E_m(TyrZ) = 970 mV,[35,36] it reproduced $E_m(P_{D1})$ and $E_m(P_{D2})$ of 1100−1200 mV.[48,49] In addition, eq 1 reproduced $E_m(P_{D1}) < E_m(P_{D2})$,[50,51] which is consistent with the experimentally measured larger $P_{D1}^{\bullet+}$ population than $P_{D2}^{\bullet+}$.[52−54] Furthermore, eq 1 yielded $E_m(S_0/S_1)$ = 730 mV,[38] which is 100 mV lower than $E_m(S_1/S_2)$ and $E_m(S_2/S_3)$: the uniquely low $E_m(S_0/S_1)$ value is consistent with the $E_m(S_0/S_1)$ value estimated previously.[35,55]

QM/MM Calculations

The unrestricted density functional theory method was employed with the B3LYP functional using the QSite program.[56] The LANL2DZ basis set is considered for Mn and Ca atoms and the 6-31G* basis set is used for other atoms (i.e., LACVP*).[57] A diffusion function was not used in the present study, as (i) no significant difference in the geometry was observed with a diffusion function[58] and (ii) the Mn sites were >25 Å away from the focusing TyrD...D2-His189 H-bond. In the present study, the Mn_4CaO_5 cluster was included in the QM region to compare the E_m values between the TyrD...D2-His189 pair and the Mn_4CaO_5 cluster. See refs 15, 17, 38, 58, 59 for the detailed electronic structure of the Mn_4CaO_5 cluster.

The QM and MM regions interact via Coulombic interaction between MM charges and the QM wavefunction (electrostatic embedding QM/MM scheme) and van der Waals interaction between QM and MM atoms (both of which employ van der Waals parameters).[56] Note that the QSite's frozen-orbital methodology was not used to build the QM/MM interface. In the QM region, all of the atomic coordinates were fully relaxed (rigid convergence criterion with a self-consistent field (SCF) energy convergence threshold of 5.0×10^{-6} [hartree] and an SCF density convergence threshold of 5.0×10^{-7} [hartree]). In the MM region, the positions of the H atoms were optimized using the OPLS2005 force field,[60] while the positions of the heavy atoms were fixed.

For E_m calculations, the Mn_4CaO_5 cluster was considered to be in S_0 with antiferromagnetically coupled Mn ions; the resulting Mn oxidation states (Mn1, Mn2, Mn3, Mn4) and the magnetic spin quantum number M_s were (III, IV, III, III) and 1/2[61,62] (↑↓↑↓) (corresponding to the spin multiplicity $2S + 1 = 2$) in S_0. O1−O3 and

https://doi.org/10.1021/acsphyschemau.2c00019
ACS Phys. Chem Au 2022, 2, 423−429

O5 were considered to be unprotonated (O^{2-}) and O4 was considered to be protonated (OH^-) in S_0.[17,18,63−65] The results are likely to remain unchanged even if O1−O4 are unprotonated and O5 is protonated because the distances between the Mn_4CaO_5 cluster and TyrD are sufficiently large and nearly equal (O4...TyrD = 30 Å and O5...TyrD = 28 Å[5]). The four water ligand molecules, W1−W4, were considered to be water molecules (H_2O). The Mn_4CaO_5 geometry was obtained from our previous studies.[15,17] The initial-guess wavefunctions were obtained using the ligand field theory[66] implemented in the QSite program. The QM region was defined as the Mn_4CaO_5 cluster (including the ligand side chains of D1-Asp170, D1-Glu189, D1-His332, D1-Glu333, D1-Asp342, and CP43-Glu354, and the backbone of D1-Ala344), ligand water molecules of W1−W4, O4−water chain (W539, W538, and W393), Cl-1 binding site (Cl-1, W442, W446, and side chains of D1-Asn181 and D2-Lys317), second-sphere ligands (side chains of D1-Asp61 and CP43-Arg357), the H-bond network of TyrZ (side chains of D1-Tyr161, D1-His190, and D1-Asn298), a diamond-shaped cluster of water molecules[6] (W5, W6, and W7), and P_{D1}/P_{D2}. The MM region was defined as the entire PSII protein, as in a previous study.[38] D1-His337 was considered to be protonated,[67] whereas all other titratable groups were in the standard protonation states. See ref 38 for the QM/MM-optimized atomic coordinates.

According to Schutz and Warshel, the identification of a low-barrier H-bond is valid only if the shape of the potential energy profile of the H-bond is symmetric.[9] As H atoms are not identified in the original PSII crystal structure,[5] the QM/MM-optimized geometry is needed to analyze the potential energy profiles of the H-bond. To obtain the potential energy profiles of the O···H···N H-bond between TyrD and D2-His189, the LACVP* basis set[68] was employed if not otherwise specified. The QM region was defined as [TyrD (D2-Tyr160), D2-His189, D2-Arg294, CP47-Glu364], whereas other protein units and all cofactors were approximated by the MM force field. Note that the influence of the Mn_4CaO_5 cluster on the TyrD...D2-His189 H-bond can be approximated as the MM region (e.g., O4...TyrD = 30 Å and O5...TyrD = 28 Å[5]). The QM/MM-optimized geometry was used as the initial geometry. The H atom under investigation was moved between O and N by 0.05 Å before the geometry was optimized by constraining the O−H and H−N distances, and the energy was calculated. This procedure was repeated until the H atom reached the O and N atoms. See the Supporting Information for the atomic coordinates of the QM/MM-optimized geometry.

RESULTS AND DISCUSSION

The neutral radical TyrD-O• exists when the proton is at the D2-His189 moiety (forming singly protonated His189-NH; $O_{TyrD}...N_{D2\text{-}His189}$ = 2.75 Å, $O_{TyrD}...H...N_{D2\text{-}His189}$ = 173.5°), whereas the neutral radical His189-N• exists when the proton is at the TyrD moiety (forming TyrD-OH, $O_{TyrD}...N_{D2\text{-}His189}$ = 2.71 Å, $O_{TyrD}...H...N_{D2\text{-}His189}$ = 176.2°)[25] (Figure 2). These $O_{TyrD}...N_{D2\text{-}His189}$ are close to 2.74 Å in the crystal structure,[5] which corresponds to protonated TyrD-OH.[25]

The potential energy profile suggests that TyrD and D2-His189 form a low-barrier H-bond [TyrD-O...H...N-His189]$^-$ in response to the release of the proton from TyrD-OH...N-His189-NH (Figure 3a). The low-barrier H-bond is also observed when the potential energy profile is analyzed using other basis sets (6-31G(tm),[69] Figure S1a) or functionals (B97D,[70] Figure S2a). The low-barrier H-bond [TyrD-O...H...N-His189]$^-$ is likely to exist prior to electron transfer, as high-frequency electron nuclear double-resonance spectroscopy studies suggested that D2-His189 was already deprotonated prior to electron transfer.[71] Fourier transform infrared (FTIR) spectroscopy showed that TyrD is involved in a strong H-bond at high pH (i.e., deprotonation of the H-bond is pronounced), which is in line with the present finding of the low-barrier H-bond between TyrD and D2-His189.[72] The

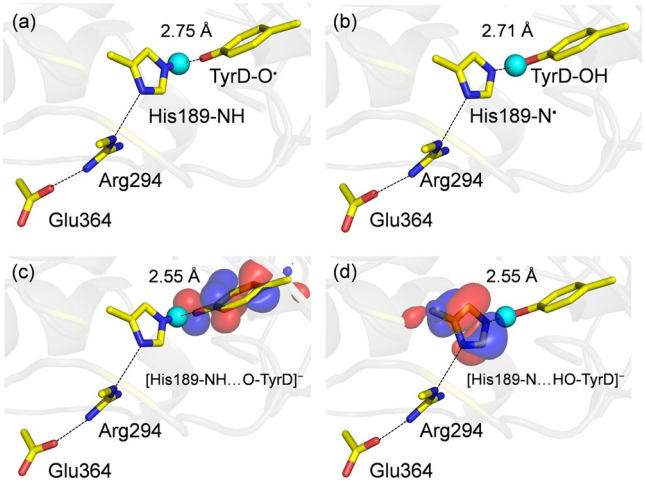

Figure 2. H-bond network of the TyrD...D2-His189 pair. (a) TyrD-O•. (b) His189-N•. (c) Low-barrier H-bond pair. H^+ is at the D2-His189 moiety. (d) Low-barrier H-bond pair. H^+ is at the TyrD moiety. Cyan balls indicate the proton along the TyrD...D2-His189 H-bond. Red and blue spheres indicate HOMO.

$O_{TyrD}...N_{D2\text{-}His189}$ distance is significantly shortened to 2.55 Å in response to the low-barrier H-bond formation. Both the H-bond distance $O_{TyrD}...N_{D2\text{-}His189}$ and the H-bond angle $O_{TyrD}...H...N_{D2\text{-}His189}$ remain at 2.55 Å and ∼180° independently of the H^+ position (e.g., 2.55 and 178.5° for [TyrD-OH...N-His189]$^-$ and 2.55 Å and 178.2° for [TyrD-O...HN-His189]$^-$), which is consistent with the features of low-barrier H-bonds.

The low-barrier H-bond formation between TyrD and D2-His189 resembles that between TyrZ and D1-His190.[6,7] However, the mechanism for the low-barrier H-bond formation differs: pK_a(TyrZ-OH/TyrZ-O$^-$) ≈ pK_a(HN-His190-NH$^+$/HN-His190-N) for the TyrZ...D1-His190 H-bond, whereas pK_a(TyrD-OH/TyrD-O$^-$) ≈ pK_a(N-His189-NH/N-His189-N$^-$) for the TyrD...D2-His189 H-bond. In the TyrZ...D1-His190 pair, a cluster of water molecules at the Mn_4CaO_5 ligand moiety donates a H-bond to TyrZ, decreasing pK_a(TyrZ) to the level of pK_a(HN-His190-NH$^+$/HN-His190-N) (∼7 in water).[6] On the other hand, anionic D2-His189 prevents TyrD-OH deprotonation, thereby increasing pK_a(TyrD) to the level of pK_a(N-His189-NH/N-His189-N$^-$) (∼14 in water[73]). Note that the difference in the histidine protonation state is due to the difference in the H-bond partner D1-Asn298, which allows D1-His190 to protonate at the Nδ site, or D2-Arg294, which does not allow D2-His189 to protonate at the Nδ site.[36]

The E_m value for [TyrD-O...H...N-His189]$^{-/\bullet}$ depends on the H^+ position along the low-barrier H-bond (Figure 3b), as observed for the low-barrier H-bond between TyrZ and D1-His190.[11] The E_m value at the TyrD moiety, E_m(TyrD-O$^{-/\bullet}$), increases as the H^+ moves toward the TyrD moiety and decreases as it moves toward the His189 moiety. The observed E_m dependence of the entire low-barrier H-bond [TyrD-O...H...N-His189]$^-$ pair on the H^+ position ultimately originates from E_m(N-His-N$^{\bullet/-}$) = ∼790 mV in water,[7,74] which is ∼100 mV higher than E_m(Tyr-O$^{\bullet/-}$) (= 680 mV[39]). These results confirm that the H^+ transfer of only ∼0.4 Å can alter E_m by ∼100 mV (Figure 3b) in low-barrier H-bonds.[11]

Figure 3b shows that E_m(TyrD-O$^{-/\bullet}$) = 670 mV and E_m(His189-N$^{-/\bullet}$) = 970 mV when the H^+ is at the D2-His189

https://doi.org/10.1021/acsphyschemau.2c00019
ACS Phys. Chem Au 2022, 2, 423−429

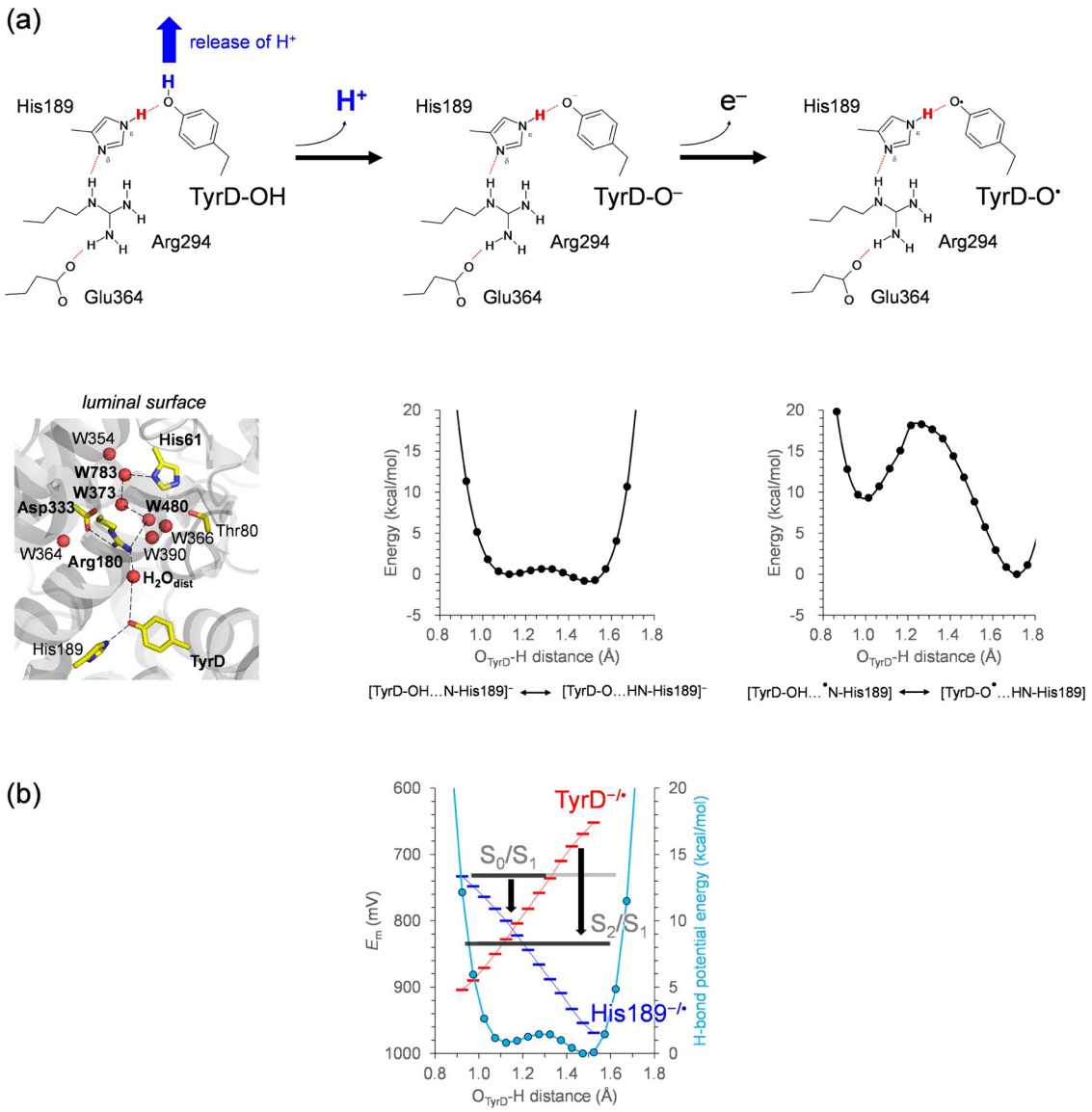

Figure 3. Proton-coupled electron transfer via TyrD. (a) Potential-energy profile of the H-bond for $[TyrD\text{-}O\ldots H\ldots N\text{-}His189]^{-}$ and $[TyrD\text{-}O\ldots H\ldots N\text{-}His189]^{\bullet}$. The left panels indicate the proton transfer pathway from TyrD toward the protein bulk surface.[25−27] Note that each conformation (black closed circle) is the QM/MM-optimized geometry. (b) Shifts in the cofactor E_m values in response to the H^+ migration along the TyrD...D2-His189 H-bond. Vertical arrows indicate electron transfer. Black horizontal lines indicate the "redox-active" H^+ positions, which facilitate electron transfer in the S_0 to S_1 oxidation and S_2 to S_1 reduction.

moiety; $E_m(TyrD\text{-}O^{-/\bullet})$ (= 830 mV) is close to E_m(His189-$N^{-/\bullet}$) (= 800 mV) when the H^+ is at the TyrD moiety. As $E_m(S_0/S_1)$ = ∼700 mV,[35,38] the TyrD...D2-His189 pair can serve as an electron acceptor for S_0 during the oxidation of S_0 to S_1 in the dark (dark adaptation) (Figure 3b). The similar E_m values suggest that the two moieties can substantially and cooperatively serve as an electron acceptor from S_0/S_1. Even if $E_m(S_0/S_1)$ was lower (e.g., −100 mV estimated by Amin et al.[75]), the TyrD...D2-His189 pair could serve as an electron acceptor for S_0.

On the other hand, the TyrD...D2-His189 pair can also serve as an electron acceptor for S_2 during the rapid decay of S_2 to S_1 in the dark,[21,31,32] as $E_m(S_2/S_1)$ = 830 mV[38] is higher than E_m for the TyrD...D2-His189 pair, especially when H^+ is at the D2-His189 moiety (Figure 3b). Although this does not necessarily mean that the histidine radical is involved in the electron transfer, the characteristics of the D2-His189 moiety are pronounced when the TyrD...D2-His189 H-bond serves as an electron donor to S_2/S_1.

In summary, TyrD and D2-His189 can form a low-barrier H-bond in response to the release of the proton toward the protein bulk surface (Figure 3a). The E_m value depends on the H^+ position along the low-barrier H-bond. This may explain why TyrD mediates both the S_0 to S_1 oxidation and the S_2 to S_1 reduction, serving as both an electron acceptor and an electron donor.

■ ASSOCIATED CONTENT

Supporting Information

The Supporting Information is available free of charge at https://pubs.acs.org/doi/10.1021/acsphyschemau.2c00019.

Potential energy profiles for H-bonds analyzed using the 6-31G(tm) basis set or the B97D functional (PDF)

https://doi.org/10.1021/acsphyschemau.2c00019
ACS Phys. Chem Au 2022, 2, 423−429

QM/MM-optimized atomic coordinates of TyrD-O• and His189-N• (TXT)

AUTHOR INFORMATION

Corresponding Author

Hiroshi Ishikita − *Research Center for Advanced Science and Technology, The University of Tokyo, Tokyo 153-8904, Japan; Department of Applied Chemistry, The University of Tokyo, Tokyo 113-8654, Japan;* orcid.org/0000-0002-5849-8150; Phone: +81-3-5452-5056; Email: hiro@appchem.t.u-tokyo.ac.jp; Fax: +81-3-5452-5083

Authors

Manoj Mandal − *Department of Chemical, Biological & Macro-Molecular Sciences, S. N. Bose National Centre for Basic Sciences, Kolkata 700106 West Bengal, India;* orcid.org/0000-0003-0184-3168

Keisuke Saito − *Research Center for Advanced Science and Technology, The University of Tokyo, Tokyo 153-8904, Japan; Department of Applied Chemistry, The University of Tokyo, Tokyo 113-8654, Japan;* orcid.org/0000-0002-2293-9743

Complete contact information is available at: https://pubs.acs.org/10.1021/acsphyschemau.2c00019

Notes

The authors declare no competing financial interest.

ACKNOWLEDGMENTS

This research was supported by JST CREST (JPMJCR1656 to H.I.), JSPS KAKENHI (18H05155, 18H01937, 20H03217, and 20H05090 to H.I., 16H06560 and 18H01186 to K.S.), and the Interdisciplinary Computational Science Program in CCS, University of Tsukuba (to K.S.). M.M. thanks the Department of Biotechnology, Government of India, for the Ramalingaswami Re-entry Fellowship scheme.

REFERENCES

(1) Schlodder, E.; Witt, H. T. Stoichiometry of proton release from the catalytic center in photosynthetic water oxidation. *J. Biol. Chem.* **1999**, *274*, 30387−30392.

(2) Suzuki, H.; Sugiura, M.; Noguchi, T. pH dependence of the flash-induced S-state transitions in the oxygen-evolving center of photosystem II from *Thermosynechoccocus elongatus* as revealed by Fourier transform infrared spectroscopy. *Biochemistry* **2005**, *44*, 1708−1718.

(3) Noguchi, T.; Inoue, Y.; Tang, X.-S. Structural coupling between the oxygen-evolving Mn cluster and a tyrosine residue in photosystem II as revealed by Fourier transform infrared spectroscopy. *Biochemistry* **1997**, *36*, 14705−14711.

(4) Berthomieu, C.; Hienerwadel, R.; Boussac, A.; Breton, J.; Diner, B. A. Hydrogen bonding of redox-active tyrosine Z of photosystem II probed by FTIR difference spectroscopy. *Biochemistry* **1998**, *37*, 10547−10554.

(5) Umena, Y.; Kawakami, K.; Shen, J.-R.; Kamiya, N. Crystal structure of oxygen-evolving photosystem II at a resolution of 1.9 Å. *Nature* **2011**, *473*, 55−60.

(6) Saito, K.; Shen, J.-R.; Ishida, T.; Ishikita, H. Short hydrogen-bond between redox-active tyrosine Y_Z and D1-His190 in the photosystem II crystal structure. *Biochemistry* **2011**, *50*, 9836−9844.

(7) Kawashima, K.; Saito, K.; Ishikita, H. Mechanism of radical formation in the H-bond network of D1-Asn298 in photosystem II. *Biochemistry* **2018**, *57*, 4997−5004.

(8) Perrin, C. L.; Nielson, J. B. "Strong" hydrogen bonds in chemistry and biology. *Annu. Rev. Phys. Chem.* **1997**, *48*, 511−544.

(9) Schutz, C. N.; Warshel, A. The low barrier hydrogen bond (LBHB) proposal revisited: the case of the Asp... His pair in serine proteases. *Proteins: Struct., Funct., Bioinf.* **2004**, *55*, 711−723.

(10) Ishikita, H.; Saito, K. Proton transfer reactions and hydrogen-bond networks in protein environments. *J. R. Soc., Interface* **2014**, *11*, No. 20130518.

(11) Saito, K.; Mandal, M.; Ishikita, H. Redox potentials along the redox-active low-barrier H-bonds in electron transfer pathways. *Phys. Chem. Chem. Phys.* **2020**, *22*, 25467−25473.

(12) Tsujimura, M.; Tamura, H.; Saito, K.; Ishikita, H. Absorption wavelength along chromophore low-barrier hydrogen bonds. *iScience* **2022**, *25*, No. 104247.

(13) Tsujimura, M.; Ishikita, H. Identification of intermediate conformations in the photocycle of the light-driven sodium-pumping rhodopsin KR2. *J. Biol. Chem.* **2021**, *296*, No. 100459.

(14) Saito, K.; Rutherford, A. W.; Ishikita, H. Mechanism of proton-coupled quinone reduction in Photosystem II. *Proc. Natl. Acad. Sci. U.S.A.* **2013**, *110*, 954−959.

(15) Kawashima, K.; Takaoka, T.; Kimura, H.; Saito, K.; Ishikita, H. O_2 evolution and recovery of the water-oxidizing enzyme. *Nat. Commun.* **2018**, *9*, No. 1247.

(16) Saito, K.; Nakagawa, M.; Ishikita, H. pK_a of the ligand water molecules in the oxygen-evolving Mn_4CaO_5 cluster in photosystem II. *Commun. Chem.* **2020**, *3*, No. 89.

(17) Saito, K.; Rutherford, A. W.; Ishikita, H. Energetics of proton release on the first oxidation step in the water-oxidizing enzyme. *Nat. Commun.* **2015**, *6*, No. 8488.

(18) Takaoka, T.; Sakashita, N.; Saito, K.; Ishikita, H. pK_a of a proton-conducting water chain in photosystem II. *J. Phys. Chem. Lett.* **2016**, *7*, 1925−1932.

(19) Babcock, G. T.; Barry, B. A.; Debus, R. J.; Hoganson, C. W.; Atamian, M.; McIntosh, L.; Sithole, I.; Yocum, C. F. Water oxidation in photosystem II: from radical chemistry to multielectron chemistry. *Biochemistry* **1989**, *28*, 9557−9565.

(20) Diner, B. A.; Babcock, G. T. *Oxygenic Photosynthesis: The Light Reactions*, Ort, D. R.; Yocum, C. F., Eds.; Kluwer Academic Publishers: Dordrecht, Netherlands, 1996; pp 213−247.

(21) Rutherford, A. W.; Boussac, A.; Faller, P. The stable tyrosyl radical in photosystem II: why D? *Biochim. Biophys. Acta, Bioenerg.* **2004**, *1655*, 222−230.

(22) Berthomieu, C.; Hienerwadel, R. Vibrational spectroscopy to study the properties of redox-active tyrosines in photosystem II and other proteins. *Biochim. Biophys. Acta, Bioenerg.* **2005**, *1707*, 51−66.

(23) Faller, P.; Debus, R. J.; Brettel, K.; Sugiura, M.; Rutherford, A. W.; Boussac, A. Rapid formation of the stable tyrosyl radical in photosystem II. *Proc. Natl. Acad. Sci. U.S.A.* **2001**, *98*, 14368−14373.

(24) Buser, C. A.; Thompson, L. K.; Diner, B. A.; Brudvig, G. W. Electron-transfer reactions in manganese-depleted photosystem II. *Biochemistry* **1990**, *29*, 8977−8985.

(25) Saito, K.; Rutherford, A. W.; Ishikita, H. Mechanism of tyrosine D oxidation in photosystem II. *Proc. Natl. Acad. Sci. U.S.A.* **2013**, *110*, 7690−7695.

(26) Saito, K.; Sakashita, N.; Ishikita, H. Energetics of the proton transfer pathway for tyrosine D in photosystem II. *Aust. J. Chem.* **2016**, *69*, 991−998.

(27) Nakamura, S.; Noguchi, T. Infrared detection of a proton released from tyrosine Y_D to the bulk upon its photo-oxidation in photosystem II. *Biochemistry* **2015**, *54*, 5045−5053.

(28) Tommos, C.; Davidsson, L.; Svensson, B.; Madsen, C.; Vermaas, W.; Styring, S. Modified EPR spectra of the tyrosine$_D$ radical in photosystem II in site-directed mutants of *Synechocystis* sp. PCC 6803: identification of side chains in the immediate vicinity of tyrosine$_D$ on the D2 protein. *Biochemistry* **1993**, *32*, 5436−5441.

(29) Tang, X. S.; Chisholm, D. A.; Dismukes, G. C.; Brudvig, G. W.; Diner, B. A. Spectroscopic evidence from site-directed mutants of *Synechocystis* PCC6803 in favor of a close interaction between histidine 189 and redox-active tyrosine 160, both of polypeptide D2 of

the photosystem II reaction center. *Biochemistry* **1993**, *32*, 13742−13748.
(30) Suga, M.; Akita, F.; Sugahara, M.; et al. Light-induced structural changes and the site of O=O bond formation in PSII caught by XFEL. *Nature* **2017**, *543*, 131−135.
(31) Vermaas, W. F. J.; Renger, G.; Dohnt, G. The reduction of the oxygen-evolving system in chloroplasts by thylakoid components. *Biochim. Biophys. Acta, Bioenerg.* **1984**, *764*, 194−202.
(32) Styring, S.; Rutherford, A. W. In the oxygen-evolving complex of photosystem II the S_0 state is oxidized to the S_1 state by D^+ (signal II_{slow}). *Biochemistry* **1987**, *26*, 2401−2405.
(33) Babcock, G. T.; Sauer, K. Electron paramagnetic resonance Signal II in spinach chloroplasts. I. Kinetic analysis for untreated chloroplasts. *Biochim. Biophys. Acta, Bioenerg.* **1973**, *325*, 483−503.
(34) Velthuys, B. R.; Visser, J. W. M. The reactivation of EPR signal II in chloroplasts treated with reduced dichlorophenol-indophenol: Evidence against a dark equilibrium between two oxidation states of the oxygen evolving system. *FEBS Lett.* **1975**, *55*, 109−112.
(35) Vass, I.; Styring, S. pH-dependent charge equilibria between tyrosine-D and the S states in photosystem II. Estimation of relative midpoint redox potentials. *Biochemistry* **1991**, *30*, 830−839.
(36) Ishikita, H.; Knapp, E. W. Function of redox-active tyrosine in photosystem II. *Biophys. J.* **2006**, *90*, 3886−3896.
(37) Boussac, A.; Etienne, A. L. Oxido-reduction kinetics of signal II slow in tris-washed chloroplasts. *Biochem. Biophys. Res. Commun.* **1982**, *109*, 1200−1205.
(38) Mandal, M.; Kawashima, K.; Saito, K.; Ishikita, H. Redox potential of the oxygen-evolving complex in the electron transfer cascade of photosystem II. *J. Phys. Chem. Lett.* **2020**, *11*, 249−255.
(39) Tommos, C.; Babcock, G. T. Proton and hydrogen currents in photosynthetic water oxidation. *Biochim. Biophys. Acta, Bioenerg.* **2000**, *1458*, 199−219.
(40) Kawashima, K.; Ishikita, H. Energetic insights into two electron transfer pathways in light-driven energy-converting enzymes. *Chem. Sci.* **2018**, *9*, 4083−4092.
(41) Watanabe, T.; Kobayashi, M. Electrochemistry of Chlorophylls. In *Chlorophylls*, Scheer, H., Ed.; CRC Press: Boca Raton, FL, 1991; pp 287−303.
(42) Méndez-Hernández, D. D.; Tarakeshwar, P.; Gust, D.; Moore, T. A.; Moore, A. L.; Mujica, V. Simple and accurate correlation of experimental redox potentials and DFT-calculated HOMO/LUMO energies of polycyclic aromatic hydrocarbons. *J. Mol. Model.* **2013**, *19*, 2845−2848.
(43) Ishikita, H.; Saito, K. Redox potentials of quinones in aqueous solution: relevance to redox potentials in protein environments. In *Microbial Photosynthesis*, Wang, Q., Ed.; Springer Singapore: Singapore, 2020; pp 115−120.
(44) Abuabara, S. G.; Rego, L. G. C.; Batista, V. S. Influence of thermal fluctuations on interfacial electron transfer in functionalized TiO_2 semiconductors. *J. Am. Chem. Soc.* **2005**, *127*, 18234−18242.
(45) Joshi, P.; Shewale, V.; Pandey, R.; Shanker, V.; Hussain, S.; Karna, S. P. Tryptophan−gold nanoparticle interaction: a first-principles quantum mechanical study. *J. Phys. Chem. C* **2011**, *115*, 22818−22826.
(46) Mulliken, R. S. Electronic population analysis on LCAO−MO molecular wave functions. I. *J. Chem. Phys.* **1955**, *23*, 1833−1840.
(47) Saito, K.; Mandal, M.; Ishikita, H. Energetics of ionized water molecules in the H-bond network near the Ca^{2+} and Cl^- binding sites in photosystem II. *Biochemistry* **2020**, *59*, 3216−3224.
(48) Klimov, V. V.; Allakhverdiev, S. I.; Demeter, S.; Krasnovskii, A. A. Photoreduction of pheophytin in the photosystem 2 of chloroplasts with respect to the redox potential of the medium. *Dokl. Akad. Nauk SSSR* **1979**, *249*, 227−230.
(49) Rutherford, A. W.; Mullet, J. E.; Crofts, A. R. Measurement of the midpoint potential of the pheophytin acceptor of photosystem II. *FEBS Lett.* **1981**, *123*, 235−237.
(50) Ishikita, H.; Saenger, W.; Biesiadka, J.; Loll, B.; Knapp, E.-W. How photosynthetic reaction centers control oxidation power in chlorophyll pairs P680, P700, and P870. *Proc. Natl. Acad. Sci. U.S.A.* **2006**, *103*, 9855−9860.
(51) Saito, K.; Ishida, T.; Sugiura, M.; Kawakami, K.; Umena, Y.; Kamiya, N.; Shen, J.-R.; Ishikita, H. Distribution of the cationic state over the chlorophyll pair of photosystem II reaction center. *J. Am. Chem. Soc.* **2011**, *133*, 14379−14388.
(52) Rigby, S. E. J.; Nugent, J. H. A.; O'Malley, P. J. ENDOR and special triple resonance studies of chlorophyll cation radicals in photosystem 2. *Biochemistry* **1994**, *33*, 10043−10050.
(53) Diner, B. A.; Schlodder, E.; Nixon, P. J.; Coleman, W. J.; Rappaport, F.; Lavergne, J.; Vermaas, W. F. J.; Chisholm, D. A. Site-directed mutations at D1-His198 and D2-His197 of photosystem II in *Synechocystis* PCC 6803: sites of primary charge separation and cation and triplet stabilization. *Biochemistry* **2001**, *40*, 9265−9281.
(54) Okubo, T.; Tomo, T.; Sugiura, M.; Noguchi, T. Perturbation of the structure of P680 and the charge distribution on its radical cation in isolated reaction center complexes of photosystem II as revealed by Fourier transform infrared spectroscopy. *Biochemistry* **2007**, *46*, 4390−4397.
(55) Geijer, P.; Morvaridi, F.; Styring, S. The S_3 state of the oxygen-evolving complex in photosystem II is converted to the $S_2Y_Z^\bullet$ state at alkaline pH. *Biochemistry* **2001**, *40*, 10881−10891.
(56) *QSite*, version 5.8; Schrödinger, LLC: New York, NY, 2012.
(57) Mandal, M.; Saito, K.; Ishikita, H. Release of electrons and protons from substrate water molecules at the oxygen-evolving complex in photosystem II. *J. Phys. Soc. Jpn.* **2022**, *91*, No. 091012.
(58) Mandal, M.; Saito, K.; Ishikita, H. The nature of the short oxygen-oxygen distance in the Mn_4CaO_6 complex of the photosystem II crystals. *J. Phys. Chem. Lett.* **2020**, *11*, 10262−10268.
(59) Mandal, M.; Saito, K.; Ishikita, H. Two distinct oxygen-radical conformations in the X-ray free electron laser structures of photosystem II. *J. Phys. Chem. Lett.* **2021**, *12*, 4032−4037.
(60) Banks, J. L.; Beard, H. S.; Cao, Y.; et al. Integrated modeling program, applied chemical theory (IMPACT). *J. Comput. Chem.* **2005**, *26*, 1752−1780.
(61) Åhrling, K. A.; Peterson, S.; Styring, S. The S_0 state EPR signal from the Mn cluster in photosystem II arises from an isolated $S = 1/2$ ground state. *Biochemistry* **1998**, *37*, 8115−8120.
(62) Boussac, A.; Kuhl, H.; Ghibaudi, E.; Rögner, M.; Rutherford, A. W. Detection of an electron paramagnetic resonance signal in the S_0 state of the manganese complex of photosystem II from *Synechococcus elongatus*. *Biochemistry* **1999**, *38*, 11942−11948.
(63) Shimizu, T.; Sugiura, M.; Noguchi, T. Mechanism of proton-coupled electron transfer in the S_0-to-S_1 transition of photosynthetic water oxidation as revealed by time-resolved infrared spectroscopy. *J. Phys. Chem. B* **2018**, *122*, 9460−9470.
(64) Shimada, Y.; Kitajima-Ihara, T.; Nagao, R.; Noguchi, T. Role of the O4 channel in photosynthetic water oxidation as revealed by Fourier transform infrared difference and time-resolved infrared analysis of the D1-S169A mutant. *J. Phys. Chem. B* **2020**, *124*, 1470−1480.
(65) Yamamoto, M.; Nakamura, S.; Noguchi, T. Protonation structure of the photosynthetic water oxidizing complex in the S_0 state as revealed by normal mode analysis using quantum mechanics/molecular mechanics calculations. *Phys. Chem. Chem. Phys.* **2020**, *22*, 24213−24225.
(66) Vacek, G.; Perry, J. K.; Langlois, J. M. Advanced initial-guess algorithm for self-consistent-field calculations on organometallic systems. *Chem. Phys. Lett.* **1999**, *310*, 189−194.
(67) Nakamura, S.; Noguchi, T. Infrared determination of the protonation state of a key histidine residue in the photosynthetic water oxidizing center. *J. Am. Chem. Soc.* **2017**, *139*, 9364−9375.
(68) Hay, P. J.; Wadt, W. R. Ab initio effective core potentials for molecular calculations. Potentials for K to Au including the outermost core orbitals. *J. Chem. Phys.* **1985**, *82*, 299−310.
(69) Rassolov, V. A.; Pople, J. A.; Ratner, M. A.; Windus, T. L. 6-31G* basis set for atoms K through Zn. *J. Chem. Phys.* **1998**, *109*, 1223−1229.

https://doi.org/10.1021/acsphyschemau.2c00019
ACS Phys. Chem Au 2022, 2, 423−429

(70) Becke, A. D. Density-functional thermochemistry. V. Systematic optimization of exchange-correlation functionals. *J. Chem. Phys.* **1997**, *107*, 8554−8560.
(71) Chatterjee, R.; Coates, C. S.; Milikisiyants, S.; Lee, C.-I.; Wagner, A.; Poluektov, O. G.; Lakshmi, K. V. High-frequency electron nuclear double-resonance spectroscopy studies of the mechanism of proton-coupled electron transfer at the tyrosine-D residue of photosystem II. *Biochemistry* **2013**, *52*, 4781−4790.
(72) Hienerwadel, R.; Diner, B. A.; Berthomieu, C. Molecular origin of the pH dependence of tyrosine D oxidation kinetics and radical stability in photosystem II. *Biochim. Biophys. Acta, Bioenerg.* **2008**, *1777*, 525−531.
(73) Bruice, T. C.; Schmir, G. L. Imidazole catalysis. II. The reaction of substituted imidazoles with phenyl acetates in aqueous solution. *J. Am. Chem. Soc.* **1958**, *80*, 148−156.
(74) Navaratnam, S.; Parsons, B. J. Reduction potential of histidine free radicals: a pulse radiolysis study. *J. Chem. Soc., Faraday Trans.* **1998**, *94*, 2577−2581.
(75) Amin, M.; Vogt, L.; Szejgis, W.; Vassiliev, S.; Brudvig, G. W.; Bruce, D.; Gunner, M. R. Proton-coupled electron transfer during the S-state transitions of the oxygen-evolving complex of photosystem II. *J. Phys. Chem. B* **2015**, *119*, 7366−7377.

https://doi.org/10.1021/acsphyschemau.2c00019
ACS Phys. Chem Au 2022, 2, 423−429